NeuroImage: Clinical 21 (2019) 101665

Contents lists available at ScienceDirect

NeuroImage: Clinical

journal homepage: www.elsevier.com/locate/ynicl

7T MRI allows detection of disturbed cortical lamination of the medial temporal lobe in patients with Alzheimer's disease

Boyd Kenkhuis[a,b,*], Laura E. Jonkman[c], Marjolein Bulk[a,b,f], Mathijs Buijs[a], Baayla D.C. Boon[d,e], Femke H. Bouwman[d], Jeroen J.G. Geurts[c], Wilma D.J. van de Berg[c], Louise van der Weerd[a,b]

[a] Department of Radiology, Leiden University Medical Center, Leiden, the Netherlands
[b] Department of Human Genetics, Leiden University Medical Center, Leiden, the Netherlands
[c] Department of Anatomy and Neurosciences, Amsterdam Neuroscience, Amsterdam UMC, VU University Medical Center, Amsterdam, the Netherlands
[d] Department of Neurology and Alzheimer Center, Amsterdam Neuroscience, Amsterdam UMC, VU University Medical Center, Amsterdam, the Netherlands
[e] Department of Pathology, Amsterdam Neuroscience, Amsterdam UMC, VU University Medical Center, Amsterdam, the Netherlands
[f] Percuros BV, Leiden, the Netherlands

ARTICLE INFO

Keywords:
Alzheimer's disease
Magnetic resonance imaging
Myelin
Iron
Cortical lamination

ABSTRACT

Using 7T T2*-weighted imaging, we scanned post-mortem hemispheres of Alzheimer patients and age-matched controls to describe the patterns of appearance of cortical lamination on T2*-weighted MRI in the medial temporal lobe and to assess the changes in Alzheimer patients versus controls. While controls showed a hypointense line of Baillarger in the majority of the cases, appearance of cortical lamination varied to a greater extent in the Alzheimer patients. Severely distorted cortical lamination was also observed in advanced stage Alzheimer patients and presented itself as a broad hypointense inhomogeneous band, covering a large part of the cortical width. Histology indicated that the changes in the appearance of visible cortical lamination were not only associated with myelin changes, but also with diffuse cortical iron alterations and depositions. Therefore, imaging cortical lamination alterations in Alzheimer patients using T2*-weighted MRI might provide new information on involved neuroanatomical structures in an advanced neurodegenerative stage.

1. Introduction

Alzheimer's disease (AD) is the leading cause of dementia and is characterized by the pathological hallmarks amyloid-beta (Aβ) plaques and (p-)tau neurofibrillary tangles (NFT). Accumulation of NFTs better reflect disease progression than Aβ plaques and accumulation starts at the trans-entorhinal region, after which it spreads throughout the temporal lobe and other cortical regions (Braak et al., 2006; Braak and Braak, 1991). Additionally, atrophy is apparent in AD brains, and its spreading pattern has been proven to correlate with both tau deposition and neuropsychological deficits (Whitwell, 2010). Detection of brain atrophy with high-resolution MRI is therefore considered a valid marker for AD detection and progression studies (Frisoni et al., 2010).

In recent years, ultra-high field MRI has been used extensively to study the anatomy of the human brain with unprecedented detail (Edwards et al., 2018). Also, *in vivo* and post-mortem imaging studies have been performed of normal aging brains to correlate MRI contrast to the underlying anatomical structure based on histopathology. For example, several groups have succeeded in imaging the line of Gennari in the V1 with T1-weighted images (Barbier et al., 2002; Turner et al., 2008; Walters et al., 2003). Outside the visual cortex, advancement from 3T to 7T MRI has made it possible to image micro-anatomic structures including some hippocampal substructures (Kerchner et al., 2010), the layered structure of the neocortex (Barazany and Assaf, 2012) and the less easily distinguishable lines of Baillarger (Fracasso et al., 2016) using both T1-weighted and T2*-weighted contrast, as well as inversion-recovery MRI.

However, cortical lamination is not only of interest in the context of structural and functional neuroanatomy, but may also provide relevant information with regard to selective vulnerability of cortical layers and regions in neurodegenerative diseases such as AD. As the different layers of the cortex each contain a characteristic distribution of neuronal cell types and connections, including the highly myelinated lines of Baillarger (Baillarger, 1840), assessment of lamination changes might provide complementary information to atrophy. Recent *in vivo* and *ex vivo* studies already showed that layer-specific atrophy might better correlate with diagnosis of AD and mild cognitive impairment (MCI) than measurement of volumetric atrophy (Adler et al., 2018;

* Corresponding author at: Departments of Radiology and Human Genetics, Leiden University Medical Center, Albinusdreef 2, 2333 ZA Leiden, the Netherlands.
E-mail address: b.kenkhuis@lumc.nl (B. Kenkhuis).

https://doi.org/10.1016/j.nicl.2019.101665
Received 24 April 2018; Received in revised form 24 October 2018; Accepted 4 January 2019
Available online 05 January 2019

Kerchner et al., 2010, 2012). Previous work in our own group showed that in the normal frontal cortex, laminar structures could be distinguished based on high resolution 7T T2*-weighted MRI. In AD patients, the lamination was severely disrupted on MRI, which correlated with layer-specific changes in myelin architecture and iron accumulation (Bulk et al., 2018a). Also on histology, distortion of cortical lamination has been observed in patients with AD, with blurring of the architectural order proceeding from the surface to deeper cortical layers with advancement of disease (Brun and Englund, 1981). Yet, apart from these few studies in small areas of the cortex, the visibility of changes in cortical lamination in AD patients on MRI has remained unexplored.

The aim of this study was to describe the visible patterns of cortical lamination on 7T MRI in the medial temporal lobe (MTL) using post-mortem hemispheres and to assess changes in cortical lamination patterns in AD patients versus age-matched controls. We found more variety in visible cortical lamination in AD patients and severely distorted cortical lamination in selective regions of the MTL in advanced stage AD patients, which reflected myelin-associated iron alterations on histology. This indicates MRI as sensitive tool for detecting pathogenic iron-associated distortions of cortical lamination in AD patients.

2. Methods

2.1. Study design

To study the visibility of cortical lamination disturbances in AD patients, 7T MR scans of unilateral hemispheres were made of AD patients and non-neurological controls. A total of 35 subjects were included, 21 of which were AD patients and 14 age-matched and sex-matched controls (Table 1). Patients were included based on clinical presentation and diagnosis was confirmed with pathological assessment by a neuropathologist (case details can be found in Supplementary Table 1). Boundaries of the anatomical regions were defined by a neuroanatomist (WvdB) and all regions were assessed for visibility of cortical lamination and alterations on high resolution T2*-weighted scans by two independent raters (BK and WvdB). To verify the observed changes in cortical lamination, histology was performed on two AD patients and one control with a variety of presentations of cortical lamination.

2.2. Brain sample preparation

The brain samples were obtained from the Netherlands Brain Bank (NBB), Netherlands Institute for Neuroscience, Amsterdam (open access: www.brainbank.nl) and the Normal Aging Brain collection Amsterdam (NABCA), dept. of Anatomy and Neurosciences, VU University Medical centre (VUmc), Amsterdam (www.nabca.eu). All material has been collected from donors from whom a written informed consent for brain autopsy and the use of material and clinical information for research purposes had been obtained. The procedures of the NBB and departments of Anatomy and Neuroscience have been approved by the Medical Ethical Committee of VUmc. The right hemisphere was collected at autopsy and formalin-fixed (4% buffered formalin; pH 7.4) for four weeks and sent to LUMC for 7T MRI. Subsequently, the hemispheres were immersed with phosphate buffered saline (PBS) for 24 h prior to scanning, to eliminate residual formalin and partially restore MR relaxation parameters (Shepherd et al., 2009). The hemisphere was then placed in a plastic bag containing a proton-free fluid (Fomblin®, LC08, Solvay). To minimize the amount of trapped air bubbles, a vacuum was applied overnight. Before scanning, the plastic bag was sealed and fixed on a plastic plateau in the coil. For future studies, the whole MRI dataset of the hemispheres together with tissue blocks from the same brains can be obtained via the afore mentioned websites of the NBB and NABCA.

Table 1
Subject characteristics.

	Controls (n = 14)	Alzheimer's disease (n = 21)	P-value
Age of Death, mean y (range)	74.6 (59–87)	70.9 (50–96)	0.228
Male/female	6/8	12/9	0.407
Braak, median (range)	1 (0–2)	6 (4–6)	0.000*
Thal Phase, median (range)	1.25 (0–3)	5 (4–5)	0.000*
Post-mortem interval,** mean (SD)	9:54 (2:46)	6:33 (2:11)	0.002*

* Indicates a significant difference with $p < .05$.
** Period from decease until end of autopsy.

2.3. MRI acquisition and post-processing

The hemispheres were scanned on a whole-body human 7T MRI system (Philips Healthcare, Best, Netherlands) using a 32 channel multi-transit head coil. Image acquisition was performed using a 3D multi gradient echo (MGE) sequence. High resolution T2*-weighted scans were obtained with echo time (TE) = 20 ms; repetition time (TR) = 36 ms; flip angle = 10° and 0.3 × 0.3 × 0.3 mm ACQ voxel size. Due to lack of support from a surrounding skull during fixation, the shape of the hemispheres was altered. The original shape of the hemispheres was restored via registration of the T2*-weighted image on the Colin 27 Average Brain atlas, using 3D slicer. (See Supplementary Fig. 1 for an overview of a representative scanned hemisphere).

2.4. Cortical lamination evaluation in AD patients and controls

We focus on the MTL and its subregions as these regions are affected in early stage AD and show highest pathological burden for both Aβ and NFTs in advanced stage AD (Braak and Braak, 1991). The specific anatomical regions selected and segmented are the Anterior Transverse Temporal Gyrus (TTG1), Cornu Ammonis 1/2/3 (CA1/2/3), Entorhinal cortex (Ent), Fusiform Gyrus (FuG), Hippocampus (Hipp), Inferior Temporal Gyrus (ITG), Middle Temporal Gyrus (MTG), Parahippocampul Gyrus (PHG), Parasubiculum (PaS), Planum Polare (PPo), Planum Temporale (Pte), Posterior Transverse Temporal Gyrus (TTG2), Presubiculum (PrS), Subiculum (S), and the Superior Temporal Gyrus (STG)). Regions were segmented in detail by a neuro-anatomist (WvdB), with comparison to the Paxinos atlas (Maj, Paxinos Atlas of the human brain, third edition) and the protocol for manual segmentation of the medial temporal lobe in 7T MRI (Berron et al., 2017). General appearance of visible cortical lamination was evaluated and described in detail for both AD patients and controls.

2.5. Semi-quantitative evaluation of cortical lamination alterations and atrophy

A semi-quantitative scoring system consisting of four categories was developed, based on the detailed description of observed contrast and the previously used scoring criteria of cortical contrast (Bulk et al., 2018a). Criteria are exemplified in the results section (Section 3.3.1). Ten specific subregions of the MTL were semi-quantitatively scored in all hemispheres, namely the Hipp, S, Ent, PHG, FuG, ITG, MTG, STG, Pte, TTG1 and TTG2. Scoring was performed by two independent trained raters (BK and WvdB) in the same 2D section of the mid-hippocampal plane. If only part of the gyrus showed a specific characteristic cortical lamination type, the whole gyrus was scored for the highest category observed. If visibility of the cortical lamination was obscured by an artefact in the MR-image, that specific region was excluded from scoring. In case of differing scores, a consensus score was reached. For AD patients, also two additional independent raters (LJ and MB) scored all cases to verify reproducibility of the results. Additionally, each region was scored for atrophy twice by an experienced

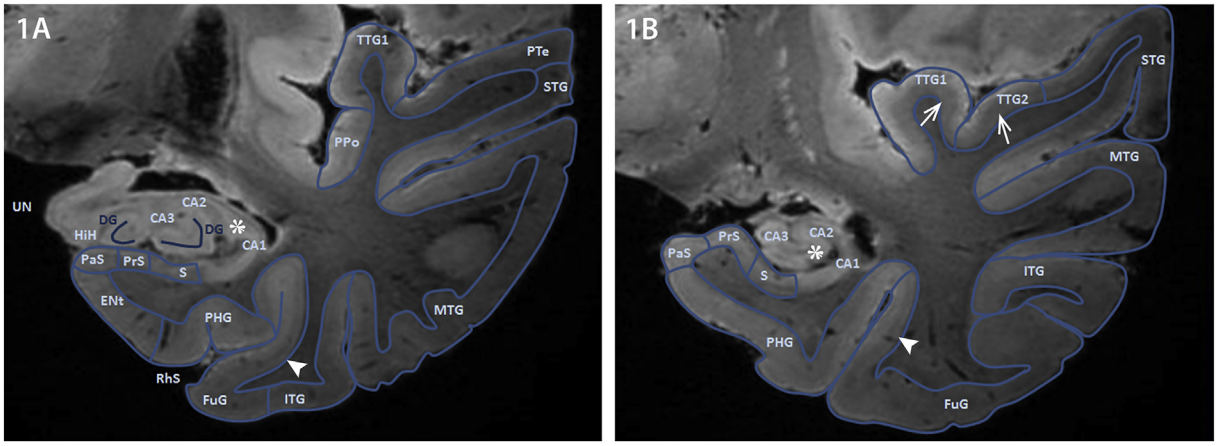

Fig. 1. Control brain segmented for the areas of interest in two coronal planes displaying the hippocampus anterior and mid; MTL subregions were segmented based on contours of the sulci and gyri and signal intensity of cortical lamination on MRI. Hyperintense band of CA3, CA2 and CA1 (Asterix, 1AB). Thin band of Baillarger (Arrowhead, 1AB). Broad band of Baillarger (Open arrows, 1B). Abbreviations: Anterior Transverse Temporal Gyrus (TTG1), Cornu Ammonis 1/2/3 (CA1/2/3) (Substructures of the Hippocampus), Dentate Gyrus (DG), Entorhinal cortex (Ent), Fascia Dentata (FD), Fusiform Gyrus (FuG), Hippocampal Head (HiH), Inferior Temporal Gyrus (ITG), Middle Temporal Gyrus (MTG), Parahippocampul Gyrus (PHG), Parasubiculum (PaS), Planum Polare (PPo), Planum Temporale (Pte), Posterior Transverse Temporal Gyrus, (TTG2), Presubiculum (PrS), Rhinal Sulcus (RhS), Subiculum (S), Superior Temporal Gyrus (STG) and Uncus (UN).

neuroanatomist (WvdB) using the common radiological scorings-scale for assessment of atrophy in dementia (Scheltens et al., 1995, 1997). Categories include normal age-related atrophy (0), mild atrophy (1), moderate atrophy (2), and severe or end-stage atrophy with enlargement of the sulci (3).

2.6. Histology and immunohistochemistry

Histological stainings were performed on the hippocampus and adjacent regions of the MTL in two AD patients with differing severities of changes in cortical lamination on MRI and one control subject. Subjects were stained for pathological hallmarks Aβ and p-Tau and for myelin and iron, which are generally considered to be the two main sources of contrast for MRI (Fukunaga et al., 2010). Tissue blocks were fixed in 4% buffered formalin, embedded in paraffin, serially cut into 6 µm, 8 µm and 20 µm thick sections and mounted on Superfrost Plus glass slides (VWR international; Leuven, Belgium). All sections were deparaffinized and dehydrated in graded series of xylene and ethanol. The 20 µm section was used for histochemical iron detection following a previously described protocol (van Duijn et al., 2013). 20-µm sections were incubated for 80 min in 1% potassium ferrocyanide, washed, followed by 100 min incubation in methanol with 0.01 M NaN3 and 0.3% H2O2. Subsequently, sections were washed with 0.1 M phosphate buffer followed by 80 min incubation in a solution containing 0.025% 3′3-diaminobenzidine-tetrahydrochloride (DAB, (DakoCytomation)) and 0.005% H2O2 in 0.1 M phosphate buffer. The reaction was stopped by washing with tap water.

The 6-to-8 µm sections were stained for myelin (anti-PLP; 1:400; Serotec, Oxford, United Kingdom), and Aβ and p-Tau (anti-abeta (6F/3D), 1:200, Dako; Anti-Tau (clone AT8), 1:200; Thermo Scientific) respectively. For the PLP and Aβ staining an antigen retrieval step was required. For the PLP the heat-induced epitope retrieval in EDTA-buffer was used at 70 °C for 30 min. For Aβ, the sections were incubated in 100% formic acid at room temperature for 15 min. Subsequently, the sections for the stains were blocked for endogenous peroxidase (0,3% H2O2 in TBS) at room temperature for 20 min. The PLP staining required a second block step at room temperature for 30 min in a block solution consisting of 3% NDS-TBS-0,5%Triton. Next, the sections were incubated with primary antibody overnight at 4 °C. After overnight incubation, the sections were incubated with biotin-labelled secondary antibodies (1:400; DAKO, Glostrup, Denmark) at room temperature (RT) for 1 h. Subsequently, sections were rinsed with TBS and incubated with streptavidin-biotin-peroxidase complex (1:400; Vectastain; Vector Laboratories Inc., Burlingame, CA, USA) at RT for 1 h. The sections were then rinsed with Tris-HCL and the peroxidase reaction was developed with 3,3′-diaminobenzidine tetrahydrochloride dihydrate (DAB; DAKO, Glostrup, Denmark) as a chromogen. Finally, sections were counterstained with haemotoxylin, dehydrated, cleared and mounted with Entallan.

2.7. Statistics

Statistics was performed on differences in patient-characteristics between AD patients and controls (Table 1). Normally distributed continuous variables (age) were compared using an independent samples *t*-test, while ordinal scales such as Braak stage and Thal phase were compared with a non-parametric Mann- Whitney *U* test. A chi-square test was used to compare categorical variables. Inter-rater agreement was calculated using Cohen's kappa statistic for all scores of cortical lamination. All statistical analyses were performed using SPSS (version 23; SPSS, Chicago, USA). A significance level of 0.05 was used.

3. Results

As the aim of this study was to provide a description of the visible cortical lamination patterns of AD patients on MRI, we started with visually assessing the observed changes, described in Sections 3.1 and 3.2. As a result of visual assessment, we found similarities in the observed alterations and grouped them accordingly. To provide a comprehensive overview of the prevalence of cortical lamination alterations in the individual regions, we consequently scored all regions of all subjects with the constructed semi-quantitative scoring system (see Section 3.3). Lastly, we verified the histological substrate, reported in Section 3.4.

3.1. Description of visibility of cortical lamination and segmentation in controls

The segmentation of the anatomical subregions within the MTL was done manually by an experienced neuroanatomist based on the location and contours of the gyri and sulci, and signal intensity on the MR images (Fig. 1). Layers of the hippocampus, such as pyramidal cell layers CA3, CA2 and CA1, could be distinguished in most cases based on contour, shape and width of the hyperintense MRI band. These layers

were visible in most controls with no or little atrophy. The boundaries between the CA3, CA2 and CA1 were difficult to determine and could only be made based on the thickness of the hyperintense band and its shape (Fig. 1, asterix). The dentate gyrus was vaguely visible in some cases. The subiculum and its subregions could be identified in most cases based on the thickness and variation of layer pattern and the so-called 'clouds' or 'clumbs'(Braak, 1978, 1980) at the outer surface. In the neocortical areas, the cortical lamination was visible as a hypointense band in the middle of the cortex. This band was seen in the majority of cases, and might correspond to the outer line of Baillarger (Fracasso et al., 2016). The entorinal and transentorinal cortex showed a pattern in most controls with a hyperintense outer layer and less intense inner layer. A similar cortical laminar profile was seen in the FuG, ITG, MTG and STG, with often one line of Baillarger visible. The visible line of Baillarger in the FuG and primarily the PHG was fairly thin and well demarcated from the other layers (Fig. 1, arrowheads). The more lateral regions including the ITG, MTG and STG showed a band of Baillarger which in some cases was broader and easier visible in comparison to the PHG. The line of Baillarger was less apparent in the Pte, but often seen in the TTG1 and TTG2, which consistently appeared to cover a larger proportion of the cortex more diffusely (Fig. 1, open arrows). The delineation of the anatomical subregions within the MTL was justified based on the shape and thickness of the cortex. Atrophy in our non-neurological controls was mild to moderate in most of the cases, which is expected considering the mean advanced age of our cohort. Severity of atrophy did not differ tremendously per area, although enthorinal cortex more often showed increased atrophy.

3.2. Description of cortical lamination in AD patients

Segmentation of the anatomical subregions in AD patients was performed based on the same characteristics as for controls. Hippocampal substructures CA3, CA2 and CA1 were still distinguishable and the transition into the subiculum was still visible. The boundaries between the CA3 to CA2 or CA2 to CA1 could not be defined based on intensity, only based thickness and location of the pyramidal cell layers. In these regions, laminar contrast was well preserved in a large proportion of cases. Hippocampal atrophy was not as pronounced in comparison to other regions, while the adjacent subiculum, showed severe atrophy. Laminar contrast in the enthorinal cortex of AD patients was only visible in a subset of cases, which coincided with extensive atrophy. However, the adjacent PHG showed consistently a preserved thin hypointense line of Baillarger, even in atrophic cases. While the controls consistently showed a line of Baillarger in the FuG, ITG, MTG, STG and Pte, the AD patients showed much more variety in visible cortical contrast. A proportion of cases still showed a line of Baillarger on MRI (Fig. 2A, B, open arrows). However interestingly, instead of a thin line of Baillarger, a much broader hypointense band was evidently visible in de middle of the grey matter, and covered more than one-third of the cortical width (Fig. 2C, D, closed arrows). Additionally, this band had a more inhomogeneous appearance with intermittent hypo- and hyperintense foci. This band was predominantly observed in the most severely atrophied AD patients and was not observed in any of the controls. Visibility of cortical lamination in the TTG1 and TTG2 on the other hand showed to be more preserved, and was comparable to the controls. Moderate to severe atrophy was present in the majority of subjects in all regions of the MTL.

3.3. Semi-quantitative evaluation of cortical alterations

3.3.1. Semi-quantitative scoring categories

Because of the changes observed during the descriptive part of this project, we grouped the observed cortical lamination patterns into four categories and scored all regions semi-quantitatively to assess frequency and spatial distribution of individual lamination patterns. The four categories for visibility of cortical lamination are: no cortical lamination (category 0), thin cortical lamination (category 1), broad cortical lamination (category 2), broad hypointense inhomogeneous band (category 3) (Fig. 3). 'No cortical lamination' is defined as one homogeneous layer with a higher signal intensity compared to the adjacent white matter. The superficial layer can have a higher signal intensity compared to the deepest layers, without an apparent hypointense band visible on MRI. The 'thin cortical lamination'-category, includes a thin well demarcated hypointense band visible in the middle of the cortex, which is considered to be the outer band of Baillarger. In the next category, 'broad cortical lamination', a similar hypointense pattern is observed as in the previous category, but the observed band covers a larger part of the cortex and merges into the more hyperintense deeper and superficial layers of the cortex more vaguely. This is suspected to be caused by a combination of contrast from both the outer, as well as inner line of Baillarger. The final category, the 'broad hypointense inhomogeneous band', is defined as an area of lower signal intensity, covering a large proportion (more than one-third) of the middle cortical layers representing distorted cortical lamination. This band is often sharply demarcated and frequently exhibits a grainy pattern with intermittent hypo- and hyperintense foci. Visually, the contrast difference of the broad hypointense inhomogeneous band and the deepest and superficial layer is also increased in comparison with the contrast observed between the hypo-intense line of Baillarger and the other layers in the other categories. This final category is generally remarkably obvious as it covers the full cortex of a specific gyrus.

As the cortical anatomy of the hippocampus and subiculum differs from the other neocortical regions in the MTL, different criteria were used to assess visibility of contrast reflecting cortical lamination. Cortical lamination was either not visible (score 0) or visible (score 1). For the hippocampus, score 1 was granted when the pyramidal layers were distinguishable from the molecular layers and the transition from CA1 to CA2 or the transition from CA1 into the subiculum was identifiable. Regarding the subiculum, if the subregions could be distinguished based on a variation of layer pattern and the so-called 'clouds' or 'clumbs' at the outer surface, lamination was considered visible (score 1). If not, the subiculum was considered to display no cortical lamination on MRI (score 0).

3.3.2. Semi-quantitative evaluation of all AD patients and controls

Results from the semi-quantitative analysis of cortical lamination in both AD patients and controls can be found in Fig. 4 and Supplementary Table 2. Regarding the controls, semi-quantitative evaluation confirmed a very consistent visible cortical laminar pattern in the hippocampus, subiculum, PHG, TTG1 and TTG2. It also showed the width and diffusivity of the band of Baillarger to be consistently greater in the TTG1 and TTG2 (category 2) compared to the PHG (category 1). Results also showed more variety in visible cortical lamination in the FuG, ITG, MTG and STG (Fig. 4A). While the FuG, which is adjacent to the PHG, predominantly showed thin cortical lamination (category 1), the ITG, MTG, STG and PTE displayed broad cortical lamination in more than half of the cases and occasionally thin cortical lamination (category 1) or no cortical lamination (category 0) was seen. The latter regions also showed a slightly increased proportion of moderately atrophic cases (Fig. 4C). A broad hypointense inhomogeneous band (category 3) was not seen in controls.

Evaluation of the AD patients showed decreased visibility of cortical lamination (category 0 instead of category 1 or 2) on MRI in regions which showed consistent laminar patterns in controls (Hipp, S, PHG, TTG1 and TTG2) (Fig. 4B). However, these regions did not show an extremely altered hypointense contrast in any of the cases. A broad hypointense inhomogeneous band (category 3) was only observed in the FuG, ITG, MTG, STG and Pte, regions which already showed more variation in visible cortical lamination in controls. This band appeared most often in the ITG and subsequently in the adjacent FuG and MTG. In few cases it also persisted into the STG and Pte (Fig. 4B). Broad cortical lamination (category 2) was the most observed cortical

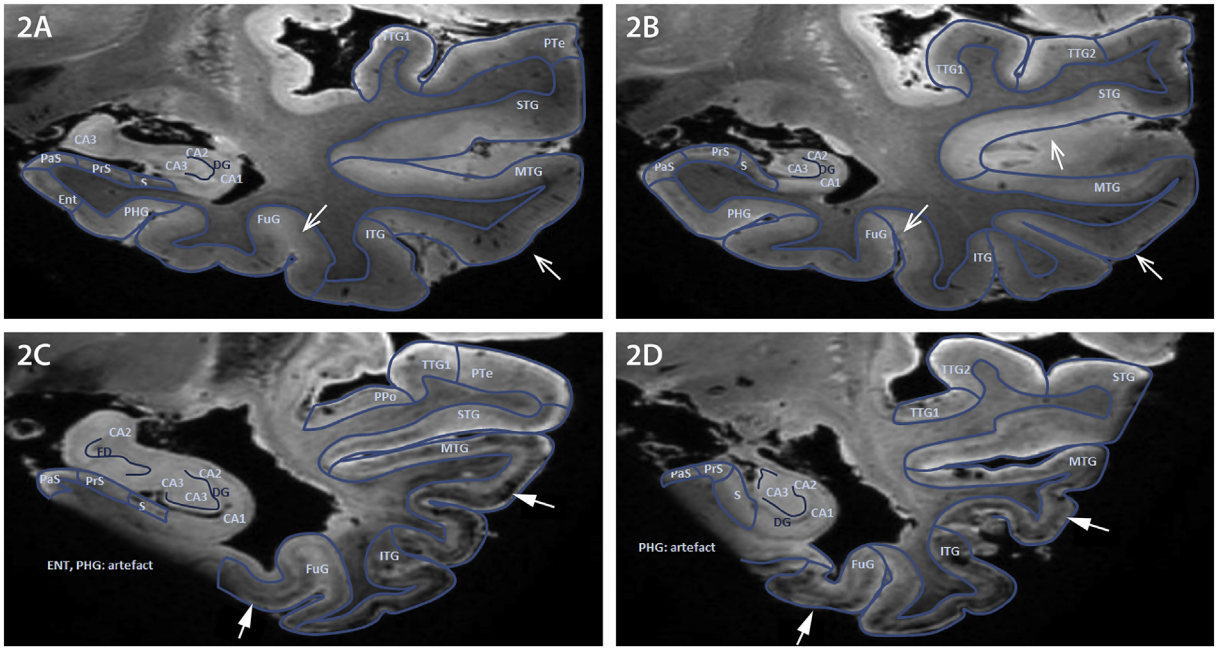

Fig. 2. Segmented images of a mildly atrophic (2A-B) and a severely atrophic (2C-D) AD hemisphere showing the anterior (2A/C) and mid (2B/D) hippocampal plane. Fig. 2A and B show a mildly affected AD hemisphere, with preserved normal cortical lamination in several regions (open arrows). Fig. 2C and D show a severely atrophic AD hemisphere with distorted cortical lamination: a broad hypointense inhomogeneous band covers a large proportion of the cortical width (closed arrows). Abbreviations: Anterior Transverse Temporal Gyrus (TTG1), Cornu Ammonis 1/2/3 (CA1/2/3) (Substructures of the Hippocampus), Dentate Gyrus (DG), Entorhinal cortex (Ent), Fascia Dentata (FD), Fusiform Gyrus (FuG), Inferior Temporal Gyrus (ITG), Middle Temporal Gyrus (MTG), Parahippocampul Gyrus (PHG), Parasubiculum (PaS), Planum Temporale (Pte), Posterior Transverse Temporal Gyrus, (TTG2), Presubiculum (PrS), Subiculum (S) and Superior Temporal Gyrus (STG).

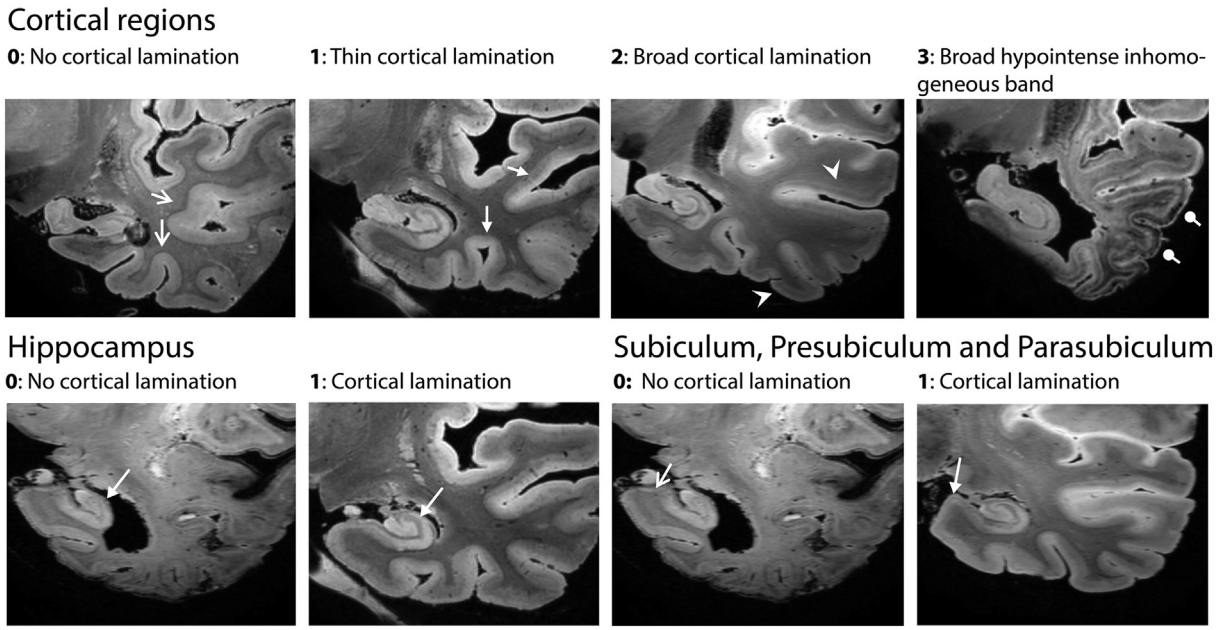

Fig. 3. Representative images of the four scoring categories for visible cortical lamination in cortical regions and the two categories for hippocampus and Subicular areas on MRI. (0) No cortical lamination was observed (open arrows). (1) Thin hypointense well-demarcated line is observed (closed arrows). (2) More broad and diffuse hypointense band is observed (arrowheads). (3) Broad hypointense inhomogeneous band is observed covering a large part of the cortical width (round arrows).

lamination pattern in these regions. All regions showing severely altered cortical lamination (category 3) showed severe or moderate atrophy (Supplementary Fig. 3) and severely altered cortical lamination only occurred in patients with Braak stage 6 (Supplementary Fig. 4), indicating distortion of cortical lamination as an end-stage event. However, in general the severely altered regions did not have more atrophy in comparison to other regions in the MTL with lesser disturbance of cortical lamination (Fig. 4D), and the spatial spreading patterns of the two pathological changes do not overlap completely.

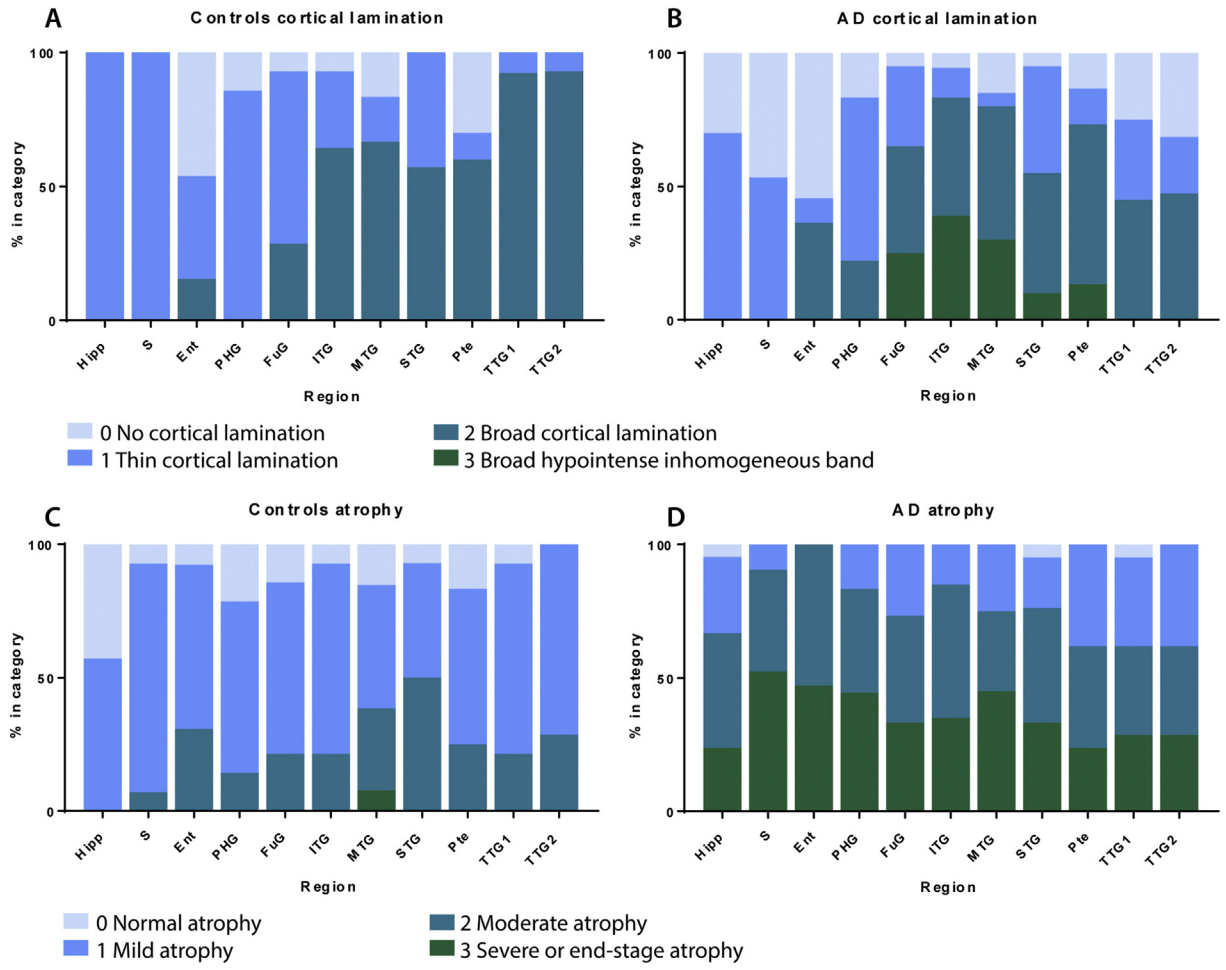

Fig. 4. Semi-quantitative scores of cortical lamination and atrophy of AD patients and controls. (A) Evaluation of cortical lamination in controls shows consistent thin- and broad cortical lamination in the Hipp/PHG and TTG1/TTG2 respectively. More variation is observed in FuG, ITG, MTG, STG and Pte. (B) The AD patients showed generally more variation and an additional distorted laminar pattern, defined as a broad hypointense inhomogeneous band in the FuG, ITG, MTG, STG and Pte. (C) Atrophy was predominantly mild to moderate in controls in all regions, (D) but more severe in AD-patients.

3.4. Histological correlation

3.4.1. Control case

In the control case neither Aβ plaques or NFTs were observed in the hippocampus and adjacent areas (Fig. 5A). Thal phase was 0 for Aβ plaques and Braak stage was 0 for NFT. On the PLP stain for myelin, the stratum lacunosum moleculare of the CA3, CA2 and CA1 was stained positively and could be distinguished from the other layers based on contrast. The (pre- and para-)subiculum showed a higher density of myelin in the superficial layer, while in the Ent and PHG a thin positive band was apparent in the middle of the cortex, which represents the band of Baillarger. As visible on the myelin stain, the band of Baillarger consists of densely myelinated fibers running tangential to the cortex. Additional to the tangential fibers, fibers running parallel to the cortex from the band of Baillarger into the more heavily myelinated white matter were also visible. The Meguro stain for iron showed a similar pattern as the myelin stain, only with less evident positive signal (Fig. 6A). Regarding the previously described cortical lamination on MRI, category 1, defined as thin cortical lamination, was visible in the Ent and PHG of the control case and this MRI-contrast closely reflected the pattern observed in both the myelin and iron stain of which the architectural order of both was preserved (Figs. 5A, 6A).

3.4.2. Moderate AD patient

The AD patient with a normal cortical lamination appearance (category 1 and 2) (Fig. 5B), was pathologically diagnosed as Thal phase 4 for Aβ and Braak stage 4 for NFTs. Many NFTs were found in the CA1, CA2, and subiculum, and a moderate amount in the CA4. In addition, the parahippocampal cortex contained neuropil threads and NFTs. The Aβ stain showed many depositions in the hippocampus with a single one in CA4. A moderate amount of Aβ plaques is also found in the neocortical areas of the PHG and FuG.

The myelin stain showed comparable immunopositive staining as the control case, with a thin line of Baillarger in the PHG and FuG. However, the iron stain showed a more pronounced positive band in the cortex compared to the control, colocalizing with the band of Baillarger in the myelin stain. Also on MRI, this band was visible as thin cortical lamination (category 1). The contrast of the band of Baillarger was more pronounced in the moderate AD patient than in the control case on MRI, likely reflecting the histologically observed increase in iron. The architectural order of myelin and iron was already a bit blurred in the Ent (Fig. 6B), which resulted in broad appearing cortical lamination on MRI (category 2).

3.4.3. Severe AD patient

The AD patient with severely distorted cortical lamination on MRI (category 3) (Fig. 5C), was pathologically diagnosed as Thal phase 5 for Aβ and Braak NFT stage 6. Additionally, this case also showed capillary amyloid angiopathy (CAA) and dysphoric amyloid angiopathy (stage 3 according to Thal). In the histological section stained for (p-)tau, abundance of NFTs was present in the FuG, PHG, Ent and subiculum. On micro-anatomic level also neuropil threads were observed in the

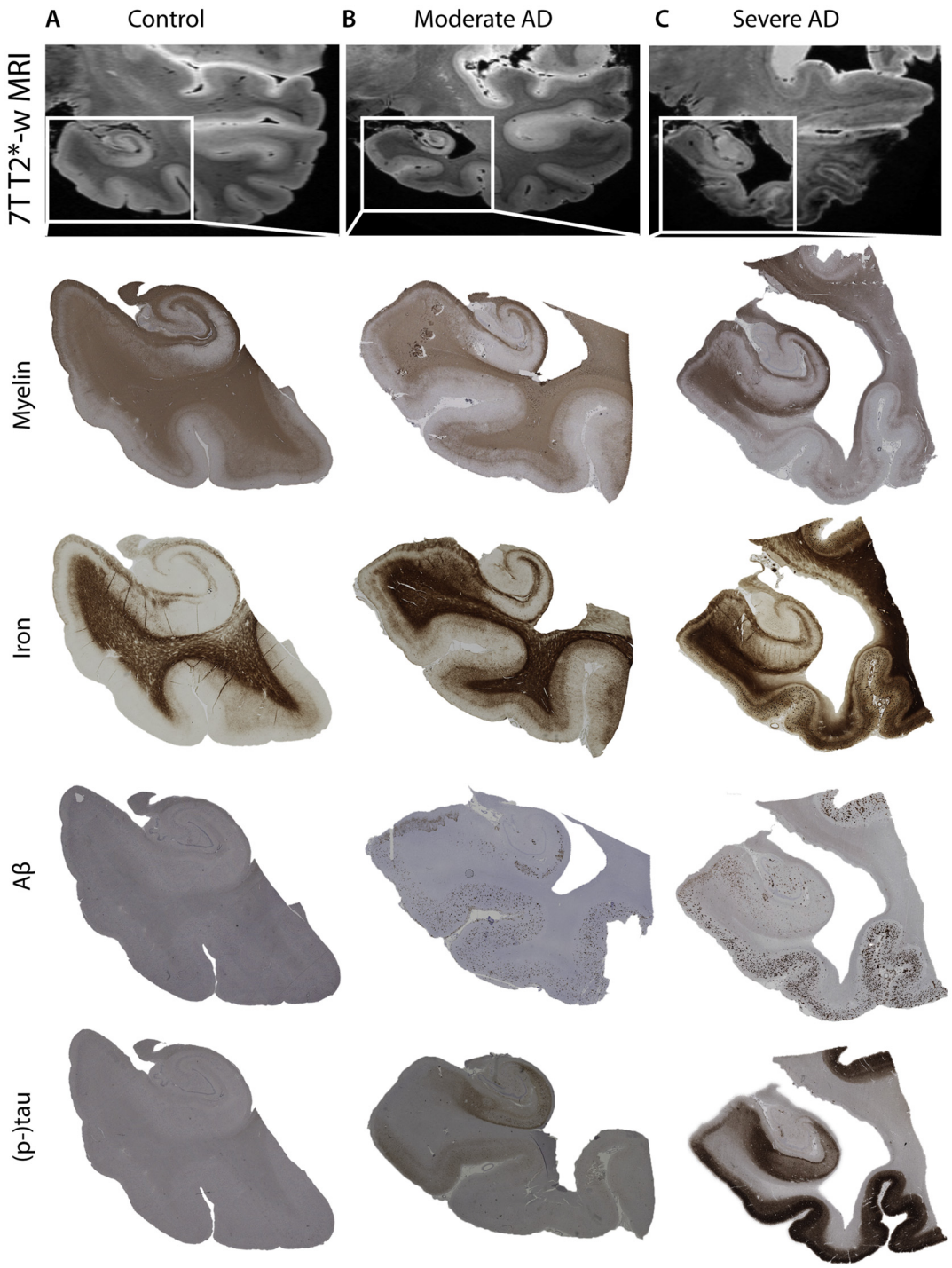

Fig. 5. Correlation of MRI with histological substrate and AD pathology. (A) Contrast of the MR-image of a control-case corresponded with myelin and iron, and no Aβ or (p-)Tau pathology was present. (B) Similar MRI contrast was observed in the moderately-affected AD-patient compared to the control, which also followed myelin and iron. Iron was already increased and also Aβ plaques and NFTs were observed. (C) Severely distorted cortical lamination was observed on MRI as a broad hypointense inhomogeneous band (category 3). MRI contrast reflected both iron deposits, co-localizing with Aβ plaques, and redistributed diffuse iron on histology in a patient with high Aβ and NFT burden.

subiculum. Some dispersed neurons with tangles are seen in CA1, but hardly in CA2–4. Regarding Aβ, some capillary angiopathy (CAA) was present in the hippocampus. An abundance of depositions was seen in the subiculum and PHG, localizing predominantly around capillaries and vessels, but none of which are classic plaques. In the PHG, also several compact depositions are present.

Myelin stain showed an affected pattern in comparison to the control case and the more mildly affected AD patient, with a more broad positive band present in the Ent, PHG,FuG and ITG (Fig. 6C). However, the most striking changes were found in the iron stain, which showed two noticeable alterations in comparison with our moderate AD and control case. First of all, an abundance of dense iron foci was visible, which seemed to correspond with the Aβ plaques in the cortex. Secondly, a broad diffuse band of iron was present in the PHG, FuG and ITG, covering more than one-third of the cortex. The broad cortical iron band and dense iron foci seem to correspond with the observed

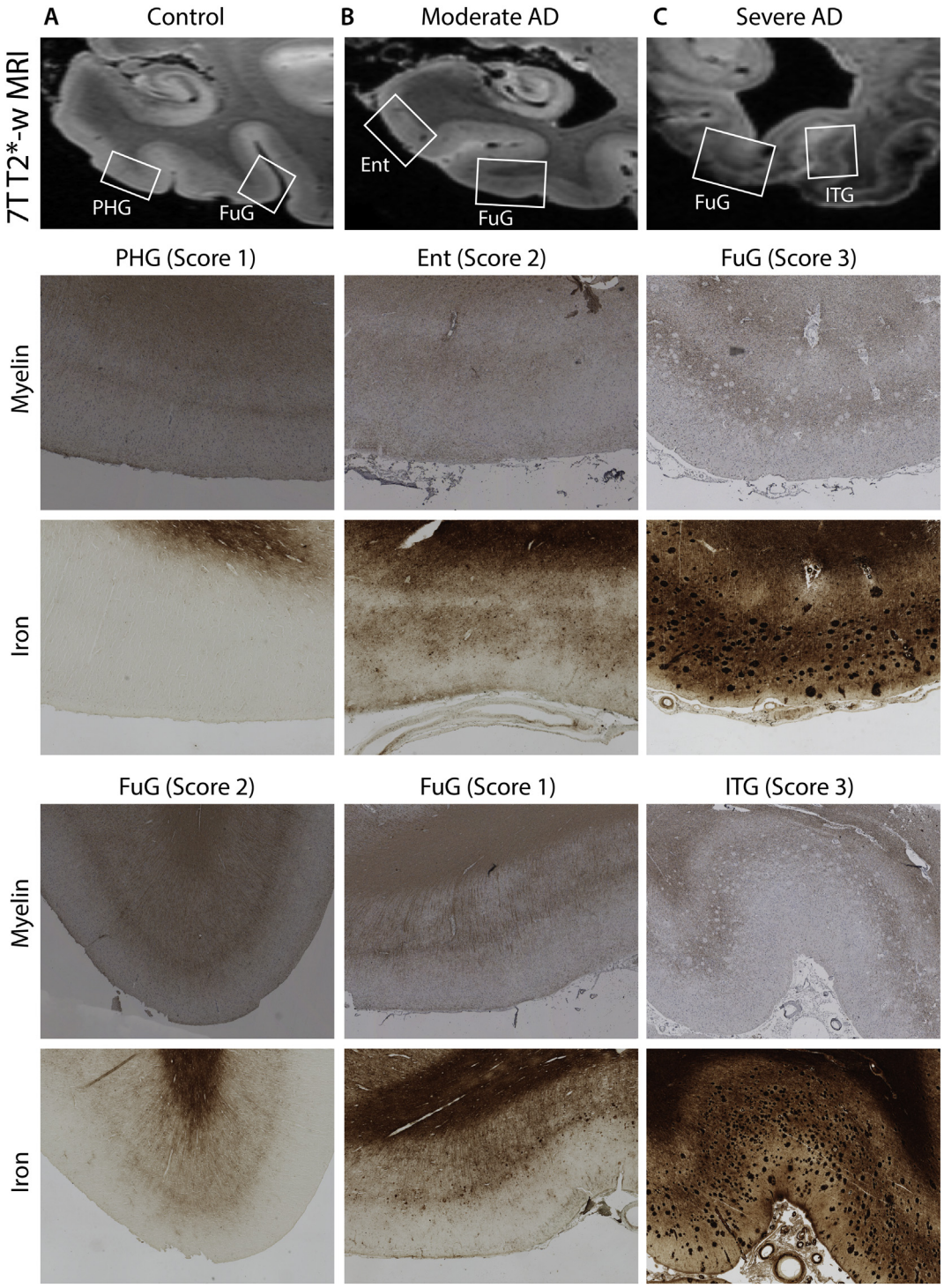

Fig. 6. Zooms of MRI corresponding histological stainings for myelin and iron. (A) Thin cortical lamination (score 1) in the PHG is reflected by a thin myelin band, but no iron band is visible. In the FuG both the iron and myelin band are increasingly visible, reflected by broad cortical lamination (score 2) on MRI. (B) Broad cortical lamination in the Ent is reflected by vague broad staining for myelin and iron, while thin cortical lamination in the FuG is in correspondence with well demarcated bands for both iron and myelin. (C) Broad hypointense inhomogenoous band in both FuG and ITG is reflected by broadened altered myelin organization and broadened, but mostly by increased iron staining with additional dense iron foci.

hypointense band and hypointense foci respectively (category 3), visible on the MRI image. The correspondence of the myelin stain with MRI was less evident in the AD patient with a broad hypointense inhomogeneous band (category 3).

3.4.4. Conclusion MRI-histology comparison

MRI-histology comparison indicates that the observed contrast on MRI inside the cortex largely reflected myelin in non-neurological controls and mildly affected AD patients. However, with pathology spreading throughout the cortex, cortical iron alterations and depositions occur. These influence the observed contrast, due to the high susceptibility of T2*-weighted imaging for iron.

4. Discussion

4.1. Summary

In this study we showed that ultra-high field T2*-weighted MRI of post-mortem hemispheres provides sufficient spatial resolution and contrast to detect cortical lamination in the MTL, both in controls and AD patients. Additionally, we were able to study the visibility of changes in myelo- and cytoarchitectonic structure associated with AD via MRI on a whole-brain scale. Cortical lamination varied to a greater extent in AD patients, and particularly in advanced stage AD, patients showed severely distorted cortical lamination in the FuG, ITG, MTG, STG and Pte. These changes corresponded with myelin-associated iron alterations.

4.2. Variation in cortical lamination

We identified a hypo-intense band in the middle of the cortex in both AD patients and controls, which represents the tangential highly myelinated fibers of the outer line of Baillarger (Baillarger, 1840; Fatterpekar et al., 2002; Fracasso et al., 2016). It was not possible to distinguish the two distinctive inner and outer lines of Baillarger, most likely due to insufficient isotropic resolution, variation in the myelo-architectonic patterns and orientation effect on T2*-weighted MRI. Parcellation of subregions of the MTL was feasible via a combination of visible cortical myelo- and cytoarchitecture, cortical thickness and anatomical orientation of the sulci in 3D scans. Visible cortical lamination by itself was not sufficient to parcellate subregions in 3D T2*-weighted MRI, due to variation in the observed myelinated pattern. Predominantly in controls, a thin or broad hypointense line of Baillarger was observed (category 1 or 2). Hipp/PHG and TTG1/TTG2 showed consistently thin and broad cortical myelination respectively. However, the FuG, ITG, MTG, STG and Pte were more variable in controls. In the AD patients, the variation in these regions was even more pronounced, and was also more variable in the Hipp/PHG and TTG1/TTG2. Additionally, some cases also showed extremely distorted cortical lamination on MRI in these regions, represented by a broad hypointense inhomogeneous band. A hypothesis for the observed region-specific variation in cortical lamination is that these cortical regions have the most protracted myelin development, and are therefore most vulnerable to a progressive pattern of myelin breakdown later in life (Bartzokis, 2004).

4.3. Origin of visible contrast

Although the exact origin of laminar contrast remained disputed for decades (Eickhoff et al., 2005), recent studies have indicated that T1 is strongly dependent on the lipid concentration associated with myelin (Leuze et al., 2017; Lutti et al., 2014; Sereno et al., 2013) and T2*-weighted imaging is predominantly susceptible to iron (Fukunaga et al., 2010; Stüber et al., 2014). However, the relative contribution of different biological components remains incompletely understood, and combinations of complementary quantitative images are necessary to model independent myelin and iron maps, as the distribution of iron and myelin overlap significantly (Edwards et al., 2018; Stüber et al., 2014). As a result of this overlap, both T1 and T2*-weighted imaging have shown good correspondence of contrast intensity with histological myeloarchitecture (Eickhoff et al., 2005; Fracasso et al., 2016; Stüber et al., 2014). This significant overlap is not surprising if you consider that oligodendrocytes, the myelin-forming cells, are the predominant iron-containing cells in the brain (Connor and Menzies, 1996). On our images, the observed thin and broad cortical lamination (category 1 or 2) correspond to the highly myelinated lines of Baillarger. Additionally, our histological stainings confirm that the observed hypointense band on MRI correlates with the presence of both myelin and iron, and confirm previous observations by Fukunaga et al., who showed similar laminar distribution of iron and myelin (Fukunaga et al., 2010). Therefore, colocalization of iron with myelin probably explains the sensitivity of our T2*-weighted images to the myelinated tangential fibers in the cortex, appearing as a hypointense band on MRI.

AD is known to be associated with changes in cortical iron (van Duijn et al., 2017). We previously showed disorganization of the myelin architecture in the frontal cortex of AD patients, especially in patients who develop the disease before the age of 65, also called early-onset AD (Bulk et al., 2018a). In the study by Bulk et al., the altered cortical MRI contrast observed in the AD patients, described as a diffuse hypointense band, reflects both focal iron deposits inside the Aβ plaques and redistribution of diffuse iron associated with myelin disorganization. This confirmed two already published papers reporting the sensitivity of T2*-weighted MRI for iron depositions inside Aβ plaques (Meadowcroft et al., 2009; Nabuurs et al., 2011). Also in the current study, the histological stainings of the severely affected AD patient confirm large iron deposits inside Aβ plaques and a broad diffuse iron band covering the cortex. No histological structural analysis of the myelin was performed, but the PLP stain for myelin showed a more diffuse band in our AD patient, which most likely reflects the underlying three-dimensional disorganization as a result of AD pathology.

4.4. Cortical lamination with respect to atrophy and pathology

We showed that severe atrophy was more frequently observed than distortions in cortical lamination (category 3). All regions which showed a broad hypointense inhomogeneous band also showed moderate to severe atrophy. This corresponds with literature from Brun and Englund that blurring of the cortical layers only occurs in advanced stages of AD (Brun and Englund, 1981). However, only the FuG, ITG, MTG, STG and Pte showed distorted cortical lamination, while the other regions were also often severely atrophied. This indicates an independent and disconnected spreading pattern of pathology and cortical lamination alterations. The histological stainings for Aβ and NFTs showed higher pathological burden for both hallmarks in the AD patient which showed distorted architectural layering. Again, this confirms laminar distortion as characteristic of degeneration which occurs in advanced stage AD. However, the temporal relationship of cortical lamination distortions with Aβ and Tau pathology cannot be elucidated from this study.

4.5. Limitations

A limitation of this study was that all results were based on visual assessment with a semi-quantitative scoring scale. However, a quantitative approach in our study would have been more limiting as we scored for a combination of width, distribution and inhomogeneity of contrast. Changes are apparent to trained raters, yet difficult to translate to image analysis software such as texture analysis (Hwang et al., 2016). A factor which also complicated the scoring was the variance in visibility of cortical contrast along one gyrus and in different anatomical planes. To consistently evaluate all cases, raters scored the different areas in the exact identical plane of view, were trained prior to scoring and reached a consensus in case of differing scores. Additionally, two independent raters (WB and LJ) scored all AD cases using the scoring scale, to verify reproducibility of the results. There scores are also available in Supplementary Table 2, and kappa values for inter-rater agreement with the consensus score is provided. Their kappa's were respectively 0.471 and 0.404, which is considered moderate agreement. Reflecting on these results, we expect the interrater agreement can be further improved by more rigorous training of the raters.

Secondly, histology was only performed in three representative cases and no systems to assure imaging-histology correspondence (e.g. custom-molds) were used. However, the correlations found in this article were in concordance with our previously performed extensive

MRI-histology studies using smaller tissue blocks discussed in Section 4.3 (Bulk et al., 2018a, 2018b).

The post-mortem interval of decease until autopsy differed significantly between controls and AD patients. Though both can be considered extremely short as the interval is below 10 h, unfortunately, we do not know how the post-mortem interval would impact the MR/histology measures, and do not know of any literature reporting changes on such short timeframes. This is something to study in future work.

Finally, a downside of studying post-mortem hemispheres is that longitudinal follow-up of the patients is not possible. Therefore the timeframe in which these distortions become visible on MRI with respect to other degenerative characteristics such as atrophy, remains to be elucidated. In order to accurately determine the temporal relationship between atrophy and cortical laminar distortions, in vivo studies should be performed. Nevertheless, in this cross-sectional study, severity of disease differs among the AD patients (Supplementary Table 1), enabling us to determine alterations in cortical lamination as an advanced disease state occurring event.

4.6. Clinical relevance in AD

As mentioned before, studying changes in cortical lamination might provide complementary information to atrophy. We observed that atrophy and distortions in cortical lamination do not show the exact same spreading pattern. More importantly, we showed that changes in cortical lamination are accompanied by cortical iron alterations and depositions. An in vivo study using T2*-weighted MRI found an increased phase shift in the cortex of AD patients compared to controls (van Rooden et al., 2014). Later Van Rooden et al. also showed region specific differences in peak-to-peak phase shift between early-onset AD and late-onset AD patients (van Rooden et al., 2015). Although the histological substrate could not be investigated, these changes likely reflect changes in iron, which co-occur with disorganization of the cortical myelin architecture (Bulk et al., 2018a). Currently, the role of iron in the pathogenesis of AD is being discussed extensively (Peters et al., 2015) and also on a clinical scale there is increasing evidence for the detrimental role of iron in AD. Ayton et al. showed that levels in CSF ferritin were negatively associated with cognitive performed in both mild cognitive impairment (MCI) and AD subjects (Ayton et al., 2015). Also adding quantitative susceptibility mapping, a technique sensitive to iron quantities, to Aβ positron emission tomography, increased the predictive value for cognitive decline in MCI and AD patients (Ayton et al., 2017). These studies indicate the relevance of tracking changes in cortical contrast in AD patients on T2*-weighted MRI, which reflect myelin- and iron associated disorganization.

The specificity of the observed cortical lamination changes for AD remains undetermined. Unfortunately very few studies have used 7T to study changes in susceptibility on T2*-weighted MRI in neurodegenerative diseases other than AD (McKiernan and O'Brien, 2017). There have been a few studies in Huntington's Disease, which focussed on the more disease affected areas in the basal ganglia, but none in other dementias like frontal-temporal lobe dementia or Lewis body dementia.

4.7. Conclusions

In conclusion, using 7T T2*-weighted MRI it is possible to map MTL cortical lamination alterations in AD and non-neurological controls. Semi-quantitative evaluation showed more variety in visible cortical lamination in AD patients and even severely distorted cortical lamination in advanced stage patients. A combined MRI-histology approach indicated that the observed cortical MRI contrast is largely determined by myelin. However, in advanced stage AD patients, myelin associated cortical iron alterations and depositions occur, influencing the observed cortical contrast. Therefore, T2*-weighted MRI appears to be a suitable MRI sequence to study changes in the myelin- and cytoarchitecture in varying stages of AD. Its potential for the in vivo setting should be elucidated in future studies for which the current study has set the stage by defining elaborate scoring criteria based on neuroanatomy and histology.

Disclosure statement

The authors have no conflicts of interest.

Acknowledgements

The authors thank I. M. Hegeman-Kleinn and the NABCA MRI, autopsy and lab team for technical assistance, and A. J. M. Rozemuller for neuropathological diagnosis of selected cases.

Netherlands Brain Bank (Amsterdam, The Netherlands) and Normal Aging Brain Collection Amsterdam (NABCA) for supplying AD and non-neurological brain tissue respectively.

Netherlands Organization for Scientific Research (NWO), VIDI research program, project “Amyloid and vessels”, number 864.13.014.

MB was financially supported by a grant from the European Union 7th Framework Program: BrainPath (PIAPP-GA-2013–612360).

WvB was financially supported by a grant from Amsterdam Neuroscience, ZonMW Memorabel and Alzheimer Netherlands-LECMA and Roche Pharma.

Appendix A. Supplementary data

Supplementary data to this article can be found online at https://doi.org/10.1016/j.nicl.2019.101665.

References

Adler, D.H., Wisse, L.E.M., Ittyerah, R., Pluta, J.B., Ding, S.-L., Xie, L., Wang, J., Kadivar, S., Robinson, J.L., Schuck, T., Trojanowski, J.Q., Grossman, M., Detre, J.A., Elliott, M.A., Toledo, J.B., Liu, W., Pickup, S., Miller, M.I., Das, S.R., Wolk, D.A., Yushkevich, P.A., 2018. Characterizing the human hippocampus in aging and Alzheimer's disease using a computational atlas derived from ex vivo MRI and histology. Proc. Natl. Acad. Sci. U. S. A. 115, 4252–4257. https://doi.org/10.1073/pnas.1801093115.

Ayton, S., Faux, N.G., Bush, A.I., Initiative, A.D.N., 2015. Ferritin levels in the cerebrospinal fluid predict Alzheimer's disease outcomes and are regulated by APOE. Nat. Commun. 6, 6760. https://doi.org/10.1038/ncomms7760.

Ayton, S., Fazlollahi, A., Bourgeat, P., Raniga, P., Ng, A., Lim, Y.Y., Diouf, I., Farquharson, S., Fripp, J., Ames, D., Doecke, J., Desmond, P., Ordidge, R., Masters, C.L., Rowe, C.C., Maruff, P., Villemagne, V.L., Salvado, O., Bush, A.I., 2017. Cerebral quantitative susceptibility mapping predicts amyloid-β-related cognitive decline. Brain 140, 2112–2119. https://doi.org/10.1093/brain/awx137.

Baillarger, J., 1840. Recherches sur la structure de la couche corticale des circonvolutions du cerveau. Mém. Acad. Roy. Méd. 8, 149–153.

Barazany, D., Assaf, Y., 2012. Visualization of cortical lamination patterns with magnetic resonance imaging. Cereb. Cortex 22, 2016–2023. https://doi.org/10.1093/cercor/bhr277.

Barbier, E.L., Marrett, S., Danek, A., Vortmeyer, A., van Gelderen, P., Duyn, J., Bandettini, P., Grafman, J., Koretsky, A.P., 2002. Imaging cortical anatomy by high-resolution MR at 3.0T: Detection of the stripe of Gennari in visual area 17. Magn. Reson. Med. 48, 735–738. https://doi.org/10.1002/mrm.10255.

Bartzokis, G., 2004. Age-related myelin breakdown: a developmental model of cognitive decline and Alzheimer's disease. Neurobiol. Aging 25, 5–18. https://doi.org/10.1016/J.NEUROBIOLAGING.2003.03.001.

Berron, D., Vieweg, P., Hochkeppler, A., Pluta, J.B., Ding, S.-L., Maass, A., Luther, A., Xie, L., Das, S.R., Wolk, D.A., Wolbers, T., Yushkevich, P.A., Düzel, E., Wisse, L.E.M., 2017. A protocol for manual segmentation of medial temporal lobe subregions in 7 Tesla MRI. NeuroImage Clin. 15, 466–482. https://doi.org/10.1016/j.nicl.2017.05.022.

Braak, H., 1978. Pigment architecture of the human telencephalic cortex. III. Regio praesubicularis. Cell Tissue Res. 190, 509–523.

Braak, H., 1980. Architectonics of the Human Telencephalic Cortex, Studies of Brain Function. Springer Berlin Heidelberg, Berlin, Heidelberg. https://doi.org/10.1007/978-3-642-81522-5.

Braak, H., Braak, E., 1991. Neuropathological stageing of Alzheimer-related changes. Acta Neuropathol. 82, 239–259. https://doi.org/10.1007/BF00308809.

Braak, H., Alafuzoff, I., Arzberger, T., Kretzschmar, H., Del Tredici, K., 2006. Staging of Alzheimer disease-associated neurofibrillary pathology using paraffin sections and immunocytochemistry. Acta Neuropathol. 112, 389–404. https://doi.org/10.1007/s00401-006-0127-z.

Brun, A., Englund, E., 1981. Regional pattern of degeneration in Alzheimer's disease: neuronal loss and histopathological grading. Histopathology 5, 549–564. https://doi.org/10.1111/j.1365-2559.1981.tb01818.x.

Bulk, M., Abdelmoula, W.M., Nabuurs, R.J.A., van der Graaf, L.M., Mulders, C.W.H., Mulder, A.A., Jost, C.R., Koster, A.J., van Buchem, M.A., Natté, R., Dijkstra, J., van der Weerd, L., 2018a. Postmortem MRI and histology demonstrate differential iron accumulation and cortical myelin organization in early- and late-onset Alzheimer's disease. Neurobiol. Aging 62, 231–242. https://doi.org/10.1016/J.NEUROBIOLAGING.2017.10.017.

Bulk, M., Kenkhuis, B., van der Graaf, L.M., Goeman, J.J., Natté, R., van der Weerd, L., 2018b. Postmortem T2*- weighted MRI imaging of cortical iron reflects severity of Alzheimer's disease. J. Alzheimers Dis. https://doi.org/10.3233/JAD-180317.

Connor, J.R., Menzies, S.L., 1996. Relationship of iron to oligodendrocytes and myelination. Glia 17, 83–93. https://doi.org/10.1002/(SICI)1098-1136(199606)17:2<83::AID-GLIA1>3.0.CO;2-7.

van Duijn, S., Nabuurs, R.J.A., van Duinen, S.G., Natté, R., 2013. Comparison of histological techniques to visualize iron in paraffin-embedded brain tissue of patients with Alzheimer's disease. J. Histochem. Cytochem. 61, 785–792. https://doi.org/10.1369/0022155413501325.

van Duijn, S., Bulk, M., van Duinen, S.G., Nabuurs, R.J.A., van Buchem, M.A., van der Weerd, L., Natté, R., 2017. Cortical iron reflects severity of Alzheimer's disease. J. Alzheimers Dis. 60, 1533–1545. https://doi.org/10.3233/JAD-161143.

Edwards, L.J., Kirilina, E., Mohammadi, S., Weiskopf, N., 2018. Microstructural imaging of human neocortex in vivo. NeuroImage. https://doi.org/10.1016/j.neuroimage.2018.02.055.

Eickhoff, S., Walters, N.B., Schleicher, A., Kril, J., Egan, G.F., Zilles, K., Watson, J.D.G., Amunts, K., 2005. High-resolution MRI reflects myeloarchitecture and cytoarchitecture of human cerebral cortex. Hum. Brain Mapp. 24, 206–215. https://doi.org/10.1002/hbm.20082.

Fatterpekar, G.M., Naidich, T.P., Delman, B.N., Aguinaldo, J.G., Gultekin, S.H., Sherwood, C.C., Hof, P.R., Drayer, B.P., Fayad, Z.A., 2002. Cytoarchitecture of the human cerebral cortex: MR microscopy of excised specimens at 9.4 tesla. Am. J. Neuroradiol. 23.

Fracasso, A., van Veluw, S.J., Visser, F., Luijten, P.R., Spliet, W., Zwanenburg, J.J.M., Dumoulin, S.O., Petridou, N., 2016. Lines of Baillarger in vivo and ex vivo: Myelin contrast across lamina at 7 T MRI and histology. NeuroImage 133, 163–175. https://doi.org/10.1016/j.neuroimage.2016.02.072.

Frisoni, G.B., Fox, N.C., R Jr., J.C., Scheltens, P., Thompson, P.M., 2010. The clinical use of structural MRI in Alzheimer disease. Nat. Rev. Neurol. 6, 67–77. https://doi.org/10.1038/nrneurol.2009.215.

Fukunaga, M., Li, T.-Q., van Gelderen, P., de Zwart, J.A., Shmueli, K., Yao, B., Lee, J., Maric, D., Aronova, M.A., Zhang, G., Leapman, R.D., Schenck, J.F., Merkle, H., Duyn, J.H., 2010. Layer-specific variation of iron content in cerebral cortex as a source of MRI contrast. Proc. Natl. Acad. Sci. U. S. A. 107, 3834–3839. https://doi.org/10.1073/pnas.0911177107.

Hwang, E.-J., Kim, H.-G., Kim, D., Rhee, H.Y., Ryu, C.-W., Liu, T., Wang, Y., Jahng, G.-H., 2016. Texture analyses of quantitative susceptibility maps to differentiate Alzheimer's disease from cognitive normal and mild cognitive impairment. Med. Phys. 43, 4718–4728. https://doi.org/10.1118/1.4958959.

Kerchner, G.A., Hess, C.P., Hammond-Rosenbluth, K.E., Xu, D., Rabinovici, G.D., Kelley, D.A.C., Vigneron, D.B., Nelson, S.J., Miller, B.L., 2010. Hippocampal CA1 apical neuropil atrophy in mild Alzheimer disease visualized with 7-T MRI. Neurology 75, 1381–1387. https://doi.org/10.1212/WNL.0b013e3181f736a1.

Kerchner, G.A., Deutsch, G.K., Zeineh, M., Dougherty, R.F., Saranathan, M., Rutt, B.K., 2012. Hippocampal CA1 apical neuropil atrophy and memory performance in Alzheimer's disease. NeuroImage 63, 194–202. https://doi.org/10.1016/j.neuroimage.2012.06.048.

Leuze, C., Aswendt, M., Ferenczi, E., Liu, C.W., Hsueh, B., Goubran, M., Tian, Q., Steinberg, G., Zeineh, M.M., Deisseroth, K., McNab, J.A., 2017. The separate effects of lipids and proteins on brain MRI contrast revealed through tissue clearing. NeuroImage 156, 412–422. https://doi.org/10.1016/j.neuroimage.2017.04.021.

Lutti, A., Dick, F., Sereno, M.I., Weiskopf, N., 2014. Using high-resolution quantitative mapping of R1 as an index of cortical myelination. NeuroImage 93, 176–188. https://doi.org/10.1016/j.neuroimage.2013.06.005.

McKiernan, E.F., O'Brien, J.T., 2017. 7T MRI for neurodegenerative dementias in vivo: a systematic review of the literature. J. Neurol. Neurosurg. Psychiatry. https://doi.org/10.1136/jnnp-2016-315022. (jnnp-2016-315022).

Meadowcroft, M.D., Connor, J.R., Smith, M.B., Yang, Q.X., 2009. MRI and histological analysis of beta-amyloid plaques in both human Alzheimer's disease and APP/PS1 transgenic mice. J. Magn. Reson. Imaging. https://doi.org/10.1002/jmri.21731.

Nabuurs, R.J.A., Hegeman, I., Natté, R., van Duinen, S.G., van Buchem, M.A., van der Weerd, L., Webb, A.G., 2011. High-field MRI of single histological slices using an inductively coupled, self-resonant microcoil: Application to ex vivo samples of patients with Alzheimer's disease. NMR Biomed. https://doi.org/10.1002/nbm.1598.

Peters, D.G., Connor, J.R., Meadowcroft, M.D., 2015. The relationship between iron dyshomeostasis and amyloidogenesis in Alzheimer's disease: two sides of the same coin. Neurobiol. Dis. https://doi.org/10.1016/j.nbd.2015.08.007.

van Rooden, S., Versluis, M.J., Liem, M.K., Milles, J., Maier, A.B., Oleksik, A.M., Webb, A.G., van Buchem, M.A., van der Grond, J., 2014. Cortical phase changes in Alzheimer's disease at 7T MRI: a novel imaging marker. Alzheimers Dement. 10, e19–e26. https://doi.org/10.1016/j.jalz.2013.02.002.

van Rooden, S., Doan, N.T., Versluis, M.J., Goos, J.D.C., Webb, A.G., Oleksik, A.M., van der Flier, W.M., Scheltens, P., Barkhof, F., Weverling-Rynsburger, A.W.E., Blauw, G.J., Reiber, J.H.C., van Buchem, M.A., Milles, J., van der Grond, J., 2015. 7T T2*-weighted magnetic resonance imaging reveals cortical phase differences between early- and late-onset Alzheimer's disease. Neurobiol. Aging 36, 20–26. https://doi.org/10.1016/j.neurobiolaging.2014.07.006.

Scheltens, P., Launer, L.J., Barkhof, F., Weinstein, H.C., van Gool, W.A., 1995. Visual assessment of medial temporal lobe atrophy on magnetic resonance imaging: inter-observer reliability. J. Neurol. 242, 557–560.

Scheltens, P., Pasquier, F., Weerts, J.G.E., Barkhof, F., Leys, D., 1997. Qualitative assessment of cerebral atrophy on MRI: inter- and intra-observer reproducibility in dementia and normal aging. Eur. Neurol. 37, 95–99. https://doi.org/10.1159/000117417.

Sereno, M.I., Lutti, A., Weiskopf, N., Dick, F., 2013. Mapping the human cortical surface by combining quantitative T1 with retinotopy†. Cereb. Cortex 23, 2261–2268. https://doi.org/10.1093/cercor/bhs213.

Shepherd, T.M., Thelwall, P.E., Stanisz, G.J., Blackband, S.J., 2009. Aldehyde fixative solutions alter the water relaxation and diffusion properties of nervous tissue. Magn. Reson. Med. 62, 26–34. https://doi.org/10.1002/mrm.21977.

Stüber, C., Morawski, M., Schäfer, A., Labadie, C., Wähnert, M., Leuze, C., Streicher, M., Barapatre, N., Reimann, K., Geyer, S., Spemann, D., Turner, R., 2014. Myelin and iron concentration in the human brain: a quantitative study of MRI contrast. NeuroImage 93, 95–106. https://doi.org/10.1016/j.neuroimage.2014.02.026.

Turner, R., Oros-Peusquens, A.-M., Romanzetti, S., Zilles, K., Shah, N.J., 2008. Optimised in vivo visualisation of cortical structures in the human brain at 3 T using IR-TSE. Magn. Reson. Imaging 26, 935–942. https://doi.org/10.1016/j.mri.2008.01.043.

Walters, N.B., Egan, G.F., Kril, J.J., Kean, M., Waley, P., Jenkinson, M., Watson, J.D.G., 2003. In vivo identification of human cortical areas using high-resolution MRI: an approach to cerebral structure-function correlation. Proc. Natl. Acad. Sci. U. S. A. 100, 2981–2986. https://doi.org/10.1073/pnas.0437896100.

Whitwell, J.L., 2010. Progression of atrophy in Alzheimer's disease and related disorders. Neurotox. Res. 18, 339–346. https://doi.org/10.1007/s12640-010-9175-1.